

Ordered coalescence of Si nanocrystals in SiO₂

Y. Q. Wang,¹ R. Smirani,¹ G. G. Ross,^{1,*} and F. Schiettekatte²

¹INRS-EMT, 1650, Boulevard Lionel-Boulet, Varennes, Québec, Canada J3X 1S2

²Laboratoire René-J.A.-Lévesque, Université de Montréal, Montréal, Québec, Canada, H3C 3J7

(Received 4 March 2005; published 25 April 2005)

The microstructure of the Si nanocrystals (Si nc) has been investigated using conventional and high-resolution transmission electron microscopy (HRTEM). For most of the nanocrystals (>90%) larger than 10 nm, HRTEM observations show that they are formed by the coalescence of smaller ones. Two kinds of coalescence, one being the preferential attachments of small particles to the {111} facets of a seed nanoparticle, and the other being an ordered combination of two or more small nanocrystals with appropriate orientations, have been observed.

DOI: 10.1103/PhysRevB.71.161310

PACS number(s): 68.37.Lp, 61.46.+w, 61.72.Mm, 61.72.Nn

Si nanocrystals (Si nc) embedded in a SiO₂ matrix have attracted much interest as a candidate system to act as an efficient light emitter. Although the physical mechanism for the light emission remains unclear, a lot of progress has been made in both the preparation¹⁻⁴ and characterization³⁻⁶ of the Si nc. In order to better understand and control the physical properties of the Si nc, it is fundamental and necessary to study the main factors that affect the crystal growth and microstructure development of these nanocrystals. For the nanocrystals embedded within a matrix, the coarsening is usually attributed to Ostwald ripening,⁷ in which the crystal growth takes place by diffusion of atoms between neighboring nanocrystals. Recent studies⁸⁻¹⁰ of TiO₂ and ZnS nanocrystals growing under hydrothermal conditions have shown that the oriented attachment or coalescence plays an important role in the coarsening of nanocrystals. In addition, the coalescence of small particles by twinning was also reported in FePt nanocrystals.^{11,12} In the process of the oriented attachment or coalescence, the nanoparticles can themselves act as the building blocks for crystal growth. However, for the Si nc embedded in a matrix such as SiO₂, coalescence or oriented attachment has not been observed using high-resolution transmission electron microscopy (HRTEM).

In this Rapid Communication, we report the conventional and HRTEM observations of the Si nc produced in a SiO₂ film by ion implantation and annealing. The Si nc range from 2 to 22 nm diam., and have a peculiar size distribution with the depth of the implanted layer. For most of the nanocrystals larger than 10 nm, HRTEM observations show that they are formed by the coalescence of smaller ones. Two kinds of coalescence, one being the preferential and ordered attachments of small particles to the {111} facets of a seed nanoparticle, and the other being an ordered combination (by {111} twinning) of two or more small nanocrystals with appropriate orientations in SiO₂, have been observed. The high concentration of Si ions is essential for the coalescence.

The Si nc were produced by a high-dose (3×10^{17} cm⁻²) implantation of Si⁺ into SiO₂ film and annealing (1100 °C). For a detailed experimental procedure, see Ref. 13. The specimens for TEM examination were prepared in a cross-sectional orientation ([011] zone axis for the Si substrate) using conventional techniques of mechanical polishing and

ion thinning. Dark-field examination was carried out on a Philips CM30 microscope operating at 300 kV. HRTEM and electron energy-loss spectroscopy (EELS) were performed using a JEOL JEM 2010F scanning transmission electron microscope (STEM) operating at 200 kV and equipped with a Gatan imaging filter (GIF).

Figure 1(a) shows a typical dark-field image of the specimen, which was recorded using a (2 2 0) diffraction ring of the Si nc. From Fig. 1(a), it can be clearly seen that a layer of Si nc is embedded in the SiO₂ film, starting at a depth of about 50 nm from the surface and extending for a thickness of about 240 nm. The Si nc range from 2 to 22 nm diam., and the nanocrystals in the middle region (region II) of the layer are larger than those near the free surface (region I) or the bottom of the layer (region III). The peculiar size distribution is due to the implantation process, which can produce a Gaussian-shaped Si concentration depth profile in the SiO₂ with a peak excess concentration of Si in the middle region of the implanted layer. This is also in agreement with the simulated depth profile by using the computer code SRIM.¹⁴ To confirm the composition of these nanocrystals, EELS was carried out in the regions with and without the nanocrystals. Figure 1(b) shows the background-subtracted EELS spectra with the Si L_{2,3} edges obtained from a region with Si nc (lower panel) and from a region without Si nc (upper panel). It is known that the L_{2,3} edge of pure Si appears at about 99 eV with a peak at 100.8 eV; however, the L_{2,3} edge of SiO₂ has a small peak at 106 eV and two large peaks at 108 and 115 eV.¹⁵ The peak I (at about 100.8 eV) in the lower panel of Fig. 1(b) confirms that the composition of the nanocrystals is pure Si.

To clarify the peculiar size distribution of the Si nc in this sample, extensive HRTEM investigations were carried out. It has been found that there are no evident microstructural defects inside the Si nc smaller than 5 nm, and single twins are dominant in the Si nc with diameters from 6 to 10 nm.¹³ In this paper, we focus on the HRTEM observations of the Si nc larger than 10 nm. The Si nc are stable under the 200-kV electron beam, and the exposure time for every HRTEM image is very short (0.5 s).

Figure 2 shows an example of the coalescence originating from the attachments of small particles to the {111} facets of a tetrahedral nanocrystal. The coalesced nanocrystal consists

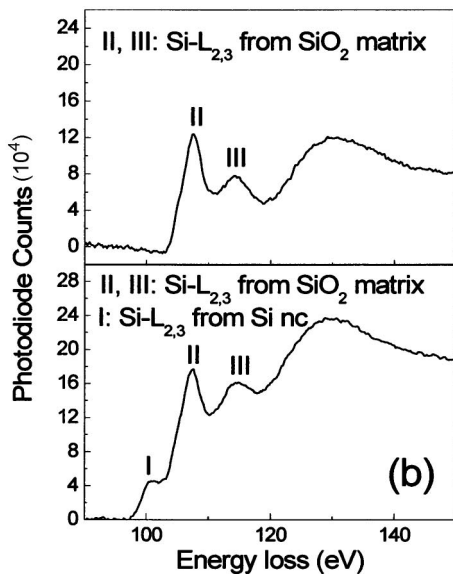
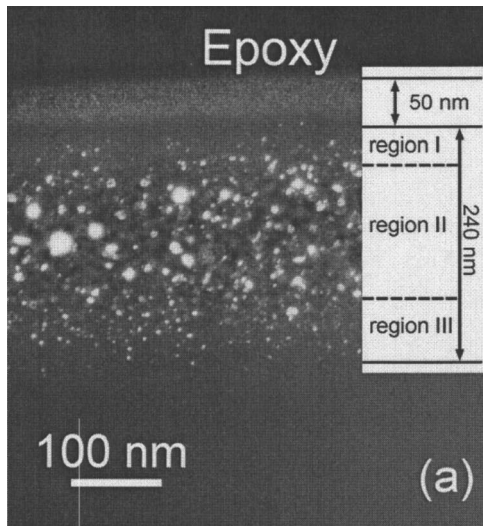


FIG. 1. (a) A typical DF image of the sample with implantation dose of $3 \times 10^{17}/\text{cm}^2$; (b) EELS spectra acquired from the regions with the Si nc and without the Si nc.

of three bigger nanograins and one smaller nanograin. When viewed along the $[011]$ direction, the nanograin (I) can be clearly seen as a triangle with facets of two $\{111\}$ planes and one (100) plane. All the nanograins are connected by $\{111\}$ twinning. The twinned-epitaxially growth of CdS nanocrystals to the $\{111\}$ facets of a tetrahedral HgS nanocrystal was also reported.^{16,17} Because the nanograin I has a high symmetry, it can act as the seed nanocrystal for the coalescence. Although the seed nanocrystal has two kinds of facets [$\{111\}$ and (100) faces], however, not all the facets are suitable for coalescence. The attachments only take place on the $\{111\}$ planes, and there is no nanograin attached to (100) plane. In nanograin II, there is an intrinsic stacking fault (indicated by the arrow labeled with SF in Fig. 2) parallel to the twinning plane $(1\bar{1}1)$. The facets of the nanograin I and shapes of the nanograins are also illustrated in Fig. 2.

Figure 3 shows another example of the coalescence originating from the attachments of small particles to a nanopar-

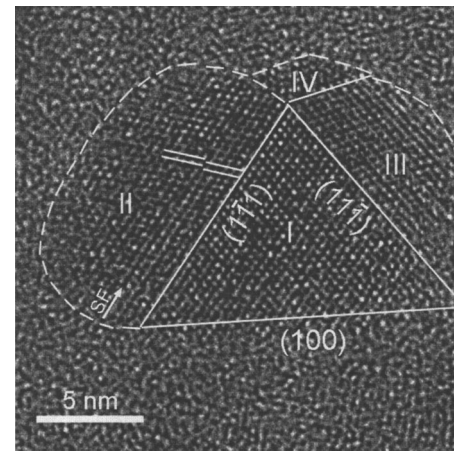


FIG. 2. HRTEM image of a coalesced nanocrystal, showing the attachments of small particles to the $\{111\}$ facets of a tetrahedral nanoparticle.

ticle with facets. In Fig. 3(a), we can see that the coalesced nanocrystal is composed of at least 10 smaller nanograins, all joined by $\{111\}$ twinning. Nanograin I has a projected shape (along the $[011]$ direction) of an approximate diamond with facets of four $\{111\}$ planes, and the coalescence is thought to take place by the attachments of the smaller nanograins to the $\{111\}$ planes of nanograin I. All the nanograins are self-

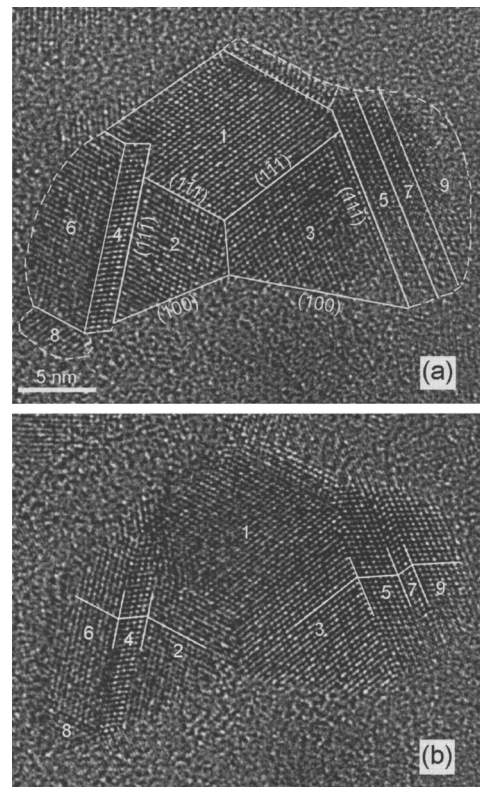


FIG. 3. (a) HRTEM image of a coalesced nanocrystal, showing the preferential and ordered attachments of small particles to the $\{111\}$ facets of an approximate-diamond-shaped nanoparticle; (b) HRTEM image of the same nanocrystal recorded under different focus condition.

arranged by twinning in an ordered way. In the middle of the coalesced nanocrystal, there is a threefold multiple twin. The triple twin has not been observed in the Si nc before, and the formation of the observed threefold multiple twin can be attributed to the coalescence of three small nanocrystals by $\{111\}$ twinning. Due to the large size of this nanocrystal, it is hard to focus the whole nanocrystal in one image at the same time. The facets and shapes of the component nanograins are also illustrated in Fig. 3(a). Figure 3(b) shows the HRTEM image of the same nanocrystal [in Fig. 3(a)] recorded under different focusing conditions. It can be clearly seen from Fig. 3(b) that nanograins 2 and 6 are connected by nanograin 4 (with six atomic planes), and nanograins 5 and 9 are joined by nanograin 7 with only four atomic planes. In addition, nanograins 6 and 8 form a single-twin boundary, and nanograins 3 and 5 also produce a single-twin boundary.

From the above HRTEM results, it is very clear that the $\{111\}$ faceting plays an important role in the coalescence of some nanoparticles. It is worth noting that only the $\{111\}$ planes are preferential for the coalescence or attachment, while there is no attachment to the (100) planes [Figs. 2 and 3(a)]. The precise role of facets on the nanoparticle surface in the coalescence process is a subject of current interest. Both experiments¹⁸ and computer simulations¹⁹ on two-dimensional islands suggest that the presence of facets can be effective in slowing down the coalescence process. Here the observed (100) facets indeed act as an obstacle for further coalescence, and the nanocrystal preferentially grows through $\{111\}$ twinning. This can explain why the morphology or shape of some nanocrystals is only elongated along one dimension. For the nanocrystals growing through Ostwald ripening, their shapes are usually spherical. Here the elongated shape of the large Si nc provides another favorable evidence for the coalescence.

Besides the observation of the coalescence originating from some nanoparticles with facets, two or more nanocrystals (without facets) in appropriate orientations are also found to be able to combine together through $\{111\}$ twinning. Figure 4 shows some examples of the coalescence of two or more nanocrystals in appropriate orientations. Figure 4(a) shows two nanocrystals (with diameter of about 5 nm) are about to combine together by twinning. An amorphous layer of SiO_x can also be seen clearly between these nanocrystals. They are both oriented along the $[011]$ direction with the $\{111\}$ planes approximately parallel to each other. This clearly shows that only those with similar orientations have better chance to coalesce. Further evidence is shown in Fig. 4(b). Figure 4(b) shows that two nanograins 1 and 3 (one smaller and the other bigger) are connected by nanograin 2 with twinning. The parallel white lines in nanograin 2 show a deviated atomic sequence, which is a characteristic for a stacking fault (SF). A closer examination of this SF shows that it belongs to an intrinsic SF. The intrinsic SF (indicated by an arrow labeled with SF) is parallel to the $\{111\}$ twinning plane. In a previous paper,¹³ a double-twin structure was reported, and it can also be regarded as a coalescence of three nanoparticles.

It is found from our HRTEM observations that all the primary nanograins are preferential to attaching or combining together by $\{111\}$ twinning. This can be explained by the

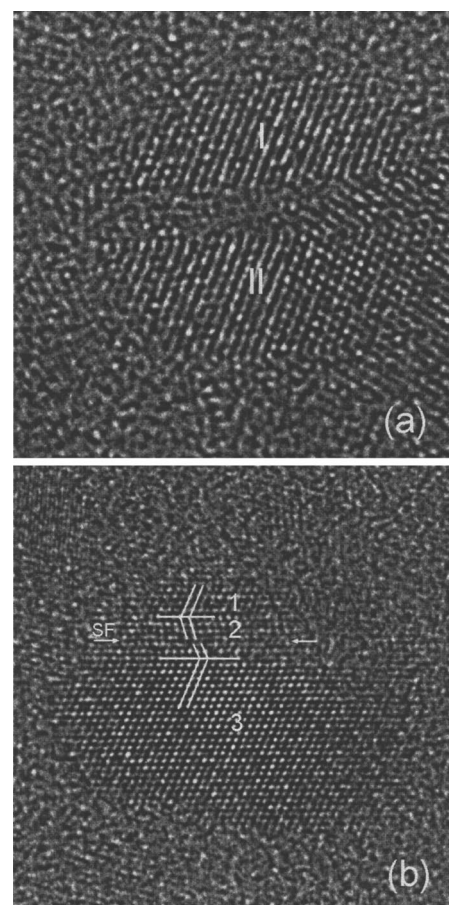


FIG. 4. HRTEM image of (a) two nanoparticles (in appropriate orientation) about to combine together; (b) the combination of three nanoparticles, showing the existence of twins and stacking fault.

energy optimization of the boundaries between the primary nanograins. In the cubic closed-packed Si crystal, the $\{111\}$ planes are the faces with the lowest surface energy ($\gamma(111) = 1.23 \text{ J/m}^2$),²⁰ so it is understandable that all the nanocrystals are coalesced *via* $\{111\}$ twinning. It was reported^{8,21} in the nanocrystals growing under hydrothermal conditions that imperfect oriented attachment or coalescence can produce defects in the coalesced crystal, which often mark the original boundaries between component nanocrystals. Here the Si nc in SiO₂ matrix exhibit a similar character for coalescence, and the twin planes in the Si nc can be regarded as the original boundaries between the component nanocrystals.

From the HRTEM analyses, it can be clearly seen that the formation of the large Si nc (dimension $>10 \text{ nm}$) is due to the coalescence of smaller ones. During the coalescence process, two or more nanoparticles combine to form a larger particle without the dissolution of any primary particle. Therefore, the growth by coalescence is controlled by the probability of contact between nanoparticles in appropriate orientations (here the primary nanoparticles are all oriented along the $[011]$ direction). This suggests that the growth by coalescence is related to the number of the initial particles with appropriate orientations in a given volume (i.e., the concentration of the nanoparticles). This is consistent with the implantation conditions (a high implantation dose of 3

$\times 10^{17} \text{ cm}^{-2}$) we used to produce the Si nc in this sample. Because the Si concentration is lower in the region near the free surface and bottom of the implanted layer, the probability for the coalescence is reduced and the growth of the small Si nc is dominated by Ostwald ripening. This could explain why the smaller Si nc mainly exist in the wings (regions I and III) while the larger ones are predominantly located in the middle region (region II) of the implanted layer, as shown in Fig. 1(a).

The effect of the annealing time and temperature on the coalescence process was also studied. In addition to 1100 °C, another two annealing temperatures (900 and 1000 °C) were also tried. It has been found that a high annealing temperature (1100 °C) is crucial for the appearance of the coalescence. For the samples annealed at lower temperatures, no evident coalescence was observed. In addition, the annealing time also plays an important role in the coalescence of the small nanoparticles. Three samples with annealing times of 5, 15, and 25 min, respectively, were studied. It has been observed that the coalescence begins in the samples with an annealing time of around 10 to 15 min, and further coalescence happens in the sample with an annealing time of 25 min. Note that only one kind of coalescence (the second

type) was observed for the samples annealed for less than 25 min. It indicates that a longer annealing time is also important for the appearance of faceting for the Si nc.

In conclusion, we present the HRTEM evidence for the coalescence of small Si nanoparticles by twinning. For most of the Si nc (>90%) larger than 10 nm, HRTEM observations show that they are formed by the coalescence of smaller ones. Two kinds of coalescence have been observed, one being the preferential and ordered attachments of small particles to the {111} facets of a seed nanocrystal, and the other being an ordered combination (by {111} twinning) of two or more small nanocrystals in appropriate orientations. All the coalesced nanocrystals have an elongated morphology. The high concentration of Si⁺ and high annealing temperature are essential for the appearance of coalescence. The long annealing time is important for the appearance of faceting.

This work has been supported by NanoQuébec and the Natural Science and Engineering Research Council of Canada (NSERC). The authors thank G. Botton and Fred Pearson from McMaster University for their assistance in the collection of EELS spectra.

*Corresponding author. Electronic address: ross@emt.inrs.ca

- ¹J. G. Zhu, C. W. White, J. D. Budai, S. P. Withrow, and Y. Chen, *J. Appl. Phys.* **78**, 4386 (1995).
- ²K. S. Min, K. V. Shcheglov, C. M. Yang, H. A. Atwater, M. L. Brongersma, and A. Polman, *Appl. Phys. Lett.* **69**, 2033 (1996).
- ³U. Kahler and H. Hofmeister, *Appl. Phys. Lett.* **75**, 641 (1999).
- ⁴T. Seto, Y. Kawakami, N. Suzuki, M. Hirasawa, and N. Aya, *Nano Lett.* **1**, 315 (2001).
- ⁵G. Franzò, S. Boninelli, D. Pacifici, F. Priolo, F. Iacona, and C. Bongiorno, *Appl. Phys. Lett.* **82**, 3871 (2003).
- ⁶F. Iacona, C. Bongiorno, C. Spinella, S. Boninelli, and F. Priolo, *J. Appl. Phys.* **95**, 3723 (2004).
- ⁷W. Ostwald, *Z. Phys. Chem., Stoechiom. Verwandtschaftsl.* **34**, 495 (1900).
- ⁸R. L. Penn and J. F. Banfield, *Geochim. Cosmochim. Acta* **63**, 1549 (1999).
- ⁹R. L. Penn and J. F. Banfield, *Science* **281**, 969 (1998).
- ¹⁰F. Huang, H. Z. Zhang, and J. F. Banfield, *Nano Lett.* **3**, 373 (2003).

- ¹¹Z. R. Dai, S. H. Sun, and Z. L. Wang, *Nano Lett.* **1**, 443 (2001).
- ¹²Z. R. Dai, S. H. Sun, and Z. L. Wang, *Surf. Sci.* **505**, 325 (2002).
- ¹³Y. Q. Wang, R. Smirani, and G. G. Ross, *Nano Lett.* **4**, 2041 (2004).
- ¹⁴J. P. Biersack and L. G. Haggmark, *Nucl. Instrum. Methods* **174**, 257 (1980).
- ¹⁵M. Takeguchi, K. Furuya, and K. Yoshihara, *Micron* **30**, 147 (1999).
- ¹⁶A. Mews, A. V. Kadavanich, U. Banin and A. P. Alivisatos, *Phys. Rev. B* **53**, R13 242 (1996).
- ¹⁷A. P. Alivisatos, *J. Phys. Chem.* **100**, 13226 (1996).
- ¹⁸W. Selke and P. M. Duxbury, *Z. Phys. B: Condens. Matter* **94**, 311 (1994).
- ¹⁹X. Yu and P. M. Duxbury, *Phys. Rev. B* **52**, 2102 (1995).
- ²⁰D. J. Eaglesham, A. E. White, L. C. Feldman, N. Moriya, and D. C. Jacobson, *Phys. Rev. Lett.* **70**, 1643 (1993).
- ²¹B. Gilbert, H. Z. Zhang, F. Huang, M. P. Finnegan, G. A. Waychunas, and J. F. Banfield, *Geochem. Trans.* **4**, 20 (2003).